Role of thermal instabilities and anomalous transport in threshold of detachment and multifacetted asymmetric radiation from the edge (MARFE)

M. Z. Tokar, F. A. Kelly, and X. Loozen
Institut für Plasmaphysik, Forschungszentrum Jülich GmbH, Association FZJ-Euratom, 52425 Jülich, Germany

(Received 8 November 2004; accepted 2 March 2005; published online 2 May 2005)

A model for the plasma edge in limiter tokamaks is elaborated, which permits us to investigate the synergy of impurity radiation, particle recycling, and edge turbulence phenomena in the formation of large-scale structures, in particular, of multifacetted asymmetric radiation from the edge. The model includes a description for the anomalous transport of charged particles induced by drift microinstabilities most typical under edge conditions. Computations show that the pattern of structures, developing when a critical plasma density is approached, is essentially determined by the poloidal inhomogeneities introduced from the Shafranov shift of magnetic surfaces and from the ballooning character of edge turbulence. © *2005 American Institute of Physics*.
[DOI: 10.1063/1.1897389]

I. INTRODUCTION

The density limit, i.e., the maximum plasma density attainable before strong deterioration of the discharge performance, is one of the most fundamental operational boundaries for fusion devices.[1] Since the fusion power scales quadratically with the density, understanding of this phenomenon is of great importance for the construction of an economical thermonuclear reactor.[2] Normally, the density limit is preceded by a significant modification of the edge plasma conditions which occurs suddenly at a critical density close to the limit. The formation of a multifacetted asymmetric radiation from the edge (MARFE), a looplike plasma structure at the high field side (HFS) with large density and small temperature, being a source of strong radiation from hydrogen neutrals and impurities, is a prominent example of such a behavior. Although the appearance of a MARFE does not universally lead to a dramatic deterioration in plasma performance, an attempt to increase the density further normally does. In other cases anomalous particle transport and convective energy losses increase dramatically when the critical conditions are reached and a poloidally symmetric radial contraction of the plasma column, detachment, takes place.

Different approaches have been proposed in order to explain the phenomena described above. Many of them involve thermal instabilities at the plasma edge which can be triggered by the specific dependence on the plasma parameters of the energy losses with impurity radiation,[3,4] plasma recycling on divertor plates,[5] or on the inner wall.[6] Another line of thinking[7] makes stress on the role of the edge microturbulence underlying anomalous losses of particle and energy from the plasma.[7–10] A strong increase of them close to the density limit is attributed to a fundamental change in the turbulence character, in particular, to the growth of low-frequency fluctuations caused by drift resistive ballooning (DRB) instability.[11]

Recently it has been demonstrated that the synergy of these processes can be of crucial importance for the density limit nature.[12] By analyzing the case of poloidally symmetric radial detachment, the anomalous transport processes and power balance were treated self-consistently. It was shown that the edge transport becomes dominated by DRB modes when the plasma density exceeds a certain critical level. As a result, the particle losses increase, the edge temperature drops strongly, and impurity radiation grows drastically, leading to a thermal instability and radiative collapse of the plasma. By considering linear instabilities, the idea to combine radiation and transport effects has been elaborated in Refs. 13 and 14.

In the present paper, we develop further the approach outlined in Ref. 12, aimed on a synergetic analysis of mechanisms responsible for the edge phenomena preceding the density limit. The tokamak magnetic geometry is taken into account through the Shafranov shift of the magnetic surfaces and the decay of the field strength with the major radius. The anomalous transport coefficients are calculated by solving numerically the eigenvalue problem for small perturbations of plasma parameters. The transport equations used now allow the variation of plasma parameters in the poloidal direction. This provides a possibility to model the formation of strongly inhomogeneous structures at the plasma edge, e.g., MARFE, and to analyze the consequences of the transition in the edge turbulence when it becomes dominated by the DRB modes and the particle and energy losses are strongly enhanced at the low field side (LFS).

Developing the model in this way permits an understanding why under certain conditions the density limit is caused by the occurrence of MARFE, but under other circumstances a transition in edge turbulence takes place.[1,8,15] In order to avoid complications in the analysis, we consider the simplest magnetic geometry with cylindrical magnetic flux surfaces nonconcentric due to Shafranov shift Δ (see Fig. 1). This geometry is specific for limiter devices like Tokamak Experiment for Technology Oriented Research

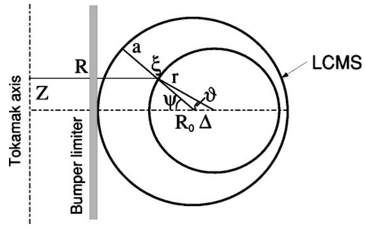

FIG. 1. The poloidal cross section of magnetic surfaces in a plasma bounded by a bumper limiter at the high field side. The coordinate systems assumed in the consideration are the following: for neutrals—the distance ξ from the point in question to the LCMS and the angle ψ between the directions from the LCMS center at R_0 to the point and to the HFS, respectively; for charged particles—the difference x between the LCMS minor radius a and that, r, of the magnetic surface with the center at $R_0+\Delta$, to which the considered point belongs, and the poloidal angle ϑ; R and Z are cylindrical coordinates.

(TEXTOR) and particular computations will be performed for the parameters typical of this device.[15,16] Only the plasma edge region just inside the last closed magnetic surface (LCMS) will be considered. It is supposed that charged particles lost by perpendicular diffusion through the LCMS into the scrape-off layer (SOL) recycle immediately back into the confined volume as neutrals on the same position at the LCMS. This approximation does not take into account the redistribution of particle flows in the SOL. The latter is, of course, important in the case of divertor geometry with X points or for a study of the effect of the clearance between the LCMS and the inner wall.[17,18] We intend to develop these aspects in a subsequent paper. This will permit the effect of plasma recycling on divertor plates on detachment and MARFE formation[5] to be accounted for.

The remainder of the paper is organized as follows. The following section describes the set of equations used for the transport of neutral and charged particles, plasma parallel momentum and heat in the edge region. Also, the boundary conditions to these equations are formulated here. In Sec. III, we deduce a set of approximate one-dimensional equations for the poloidal variation of plasma parameters averaged over the radial extension of the edge layer, derive the expressions for the components of the energy losses from the edge by particle convection, by the ionization and excitation of recycling neutrals, by impurity radiation and by plasma conduction; and analyze possible mechanisms of thermal instability due to these loss channels. In Sec. IV, the model used for the determination of anomalous transport coefficients perpendicular to the magnetic surfaces is outlined and it is demonstrated that this reproduces the strong increase in the transport and its ballooning character when the plasma collisionality exceeds a critical level.[9,10] The results of calculations with prescribed transport characteristics and with those determined from the developed transport model are presented and discussed in Sec. V. Concluding remarks are given in Sec. VI.

II. TRANSPORT EQUATIONS

A. Particle transport

The neutral particles generated on the machine walls by recombination of electrons and ions can be separated in two main fractions: (i) desorbing "cold" neutrals with the wall temperature which is much lower than the edge plasma temperature T and (ii) "hot" atoms with an energy of the order of T, which are produced by reflection of ions from the wall. In the confined plasma volume inside the LCMS, cold atoms are ionized by electrons and charge exchange with ions. The latter process together with volume recombination of charged particles, which is especially important at low temperature in MARFE region, leads to the production of additional hot neutrals. Due to ionization and charge exchange the density n_c of cold neutral particles decays with the distance from the LCMS, ξ:

$$V_c \frac{\partial n_c}{\partial \xi} = - S_c. \tag{1}$$

The subsequent charge exchange leads to random motion of hot atoms and a diffusion approximation[19–21] is used to model their density n_h:

$$\frac{\partial}{\partial \xi}\left(- D_h \frac{\partial n_h}{\partial \xi} \right) = - S_h. \tag{2}$$

In the equations above, $V_c \approx 10^3$ m/s is the velocity of cold atoms, $S_c=(k_i+k_{\mathrm{cx}})nn_c$, $S_h=k_i nn_h - k_{\mathrm{cx}} nn_c - k_r n^2$ the sinks of neutral particles with k_i, k_{cx}, k_r being the rate coefficients of ionization, charge exchange, and recombination, respectively, and n the plasma density, $D_h=T/m_a/(k_i+k_{\mathrm{cx}})/n$ is the diffusivity of atoms with mass m_a.

The diffusive approximation for hot atoms implies that their energy can be characterized by an "effective" temperature governed by the heat balance of atoms (see, e.g., Ref. 21). This assumption can be, however, questionable if the characteristic length for the ion temperature change is comparable with the penetration depth of neutrals. This is normally the case in realistic plasmas and kinetic approximation should be applied for a firm treatment. Nevertheless, the model in question provides very reasonable results for such important macroscopic characteristics as the total source of charged particles, energy losses on neutral ionization, etc. This has been demonstrated in Ref. 22 by comparing the model predictions with those from the three-dimensional (3D) code package EMC3-EIRENE.

The density of charged particles is governed by the continuity equation

$$\frac{\partial n}{\partial t} + \nabla_\perp \Gamma_\perp + \nabla_\parallel \Gamma_\parallel = S_c + S_h, \tag{3}$$

where $\Gamma_\perp = -D_\perp \nabla_\perp n$ is the component of the plasma flux density perpendicular to the magnetic surfaces, $D_\perp$ the diffusivity of charged particles; in the case of nonconcentric circular surfaces, $\nabla_\perp \approx (1/\sqrt{g_{xx}})(\partial/\partial_x)$,[23] where the metric coefficient g_{xx} takes into account the variation of the distance between neighboring magnetic surfaces with the poloidal angle ϑ, and $\nabla_\parallel = \partial\vartheta/(qR)$ for axis-symmetric configurations. Equation (3) does not include poloidal particle flows due to drifts important, in particular, for MARFE poloidal asymmetry. The corresponding development of the model will be done in future.

Strictly speaking the assumption of a diffusive nature of the perpendicular transport is actually at odds to experimental observations in which it is via convective structures with characteristic dimensions of 1 cm in the poloidal and radial directions.[11] Only, for a scale larger than this an effective average diffusive description can be introduced. Such a scale is still small compared with the characteristic dimensions in question and the adopted concept of a diffusive transport should not lead to completely irrelevant results. Nevertheless, a coupling of the present model with a turbulence code, which provides a simulation of convective structures, would significantly improve the reliability of the results.

B. Transport of plasma parallel momentum

The particle flux component parallel to the field lines, $\Gamma_\parallel$, is determined from the sum of the momentum balance equations for electrons and ions:

$$\frac{\partial\Gamma_\parallel}{\partial t} + \nabla_\parallel\left(\frac{2nT}{m_i} + \frac{\Gamma_\parallel^2}{n}\right) + \nabla_\perp\left(\frac{\Gamma_\perp\Gamma_\parallel}{n}\right) = \frac{S_h\Gamma_\parallel}{n}, \tag{4}$$

where we assume the same temperature T for both types of charged particles. This equation implies that the parallel momentum is changed by the pressure gradient, is transferred with the plasma motion in the radial direction, is lost by charge exchange with cold neutrals, which do not have any parallel velocity in average, and is gained by ionization of hot atoms, which have acquired the ion velocity before.

C. Heat transport

The plasma temperature T is governed by the sum of electron and ion heat transport equations:

$$3\frac{\partial nT}{\partial t} + \nabla_\perp q_\perp + \nabla_\parallel\left[-\kappa_\parallel\nabla_\parallel T + \Gamma_\parallel\left(5T + \frac{m_i}{2}\frac{\Gamma_\parallel^2}{n^2}\right)\right]$$
$$= \frac{3}{2}TS_h - E_i(S_c + S_h) - Q_{\rm rad}. \tag{5}$$

Here $q_\perp = 3\Gamma_\perp T - \kappa_\perp\nabla_\perp T$ is the heat flux density component perpendicular to the magnetic surfaces with both convective and conductive contributions included, $\kappa_\parallel$ and $\kappa_\perp$ are the parallel and perpendicular components of the plasma heat conductivity; in the right-hand side (RHS) the first term describes the energy gained by ions by ionization of hot neutrals and lost by charge exchange of cold ones, the second one the loss by electrons on ionization and excitation of neutrals, and the third one, $Q_{\rm rad}$, the losses with impurity radiation.

D. Boundary conditions

In the present paper we consider the case of an immediate reaction of the wall when the influx of neutrals into the plasma is always in equilibrium with the ion outflow from the plasma:

$$V_c n_c(0) = (1 - R_p)\Gamma_p, \quad -D_h\frac{\partial n_h}{\partial\xi}(0) = R_p\Gamma_p, \tag{6}$$

where R_p is the reflection coefficient of ions and $\Gamma_p \equiv -\Gamma_\perp(0)$. A finite time of the wall reaction can lead to significant changes in the dynamics of MARFE formation.[24] This phenomenon will be discussed in detail elsewhere.

In addition we assume as given, the e-folding lengths of the plasma density and temperature, δ_n and δ_T, at the LCMS, $x=0$,

$$x = 0\,\frac{\partial n}{\partial x} = \frac{n}{\delta_n}, \quad \frac{\partial T}{\partial x} = \frac{T}{\delta_T}. \tag{7}$$

They will be determined self-consistently when a model for the transport in the scrape-off layer will be included into consideration. At the interface with the plasma core, $x = \delta_{\rm edge}$, poloidal inhomogeneities in plasma profiles disappear and the plasma particle density is equal to a prescribed one; in addition, the particle fluxes vanish and heat is transported only by conduction:

$$\frac{\partial T}{\partial x} = q_{\rm core} \Bigg/ \int_0^{2\pi}\frac{\kappa_\perp}{\sqrt{g_{xx}}}\frac{d\vartheta}{2\pi}, \tag{8}$$

with $q_{\rm core} = P_{\rm core}/S_{\rm core}$, $P_{\rm core}$ being the heating power and $S_{\rm core}$ the total area of the core-edge interface surface. There are no causes for an up and down asymmetry of plasma parameters in the present problem formulation and $\partial n/\partial\vartheta = \partial T/\partial\vartheta = \Gamma_\parallel = 0$ is assumed at $\vartheta = 0, 2\pi$.

III. APPROXIMATE ONE-DIMENSIONAL MODEL

In this section we reduce the set of transport equations above to approximate one-dimensional (1D) ones. This is done by averaging the initial equations in the radial direction over the width of the edge layer, $\delta_{\rm edge}$:

$$\langle f\rangle(\vartheta) = \int_0^{\delta_{\rm edge}} f(x,\vartheta) \times \frac{dx}{\delta_{\rm edge}}.$$

Such a simplification[12,24] reduces numerical efforts significantly, but should be well validated since 1D equations are used to model an intrinsically 2D problem. Conversely to usual 1D models for the plasma edge (see, e.g., Ref. 6), the present procedure allows to fulfill the boundary conditions at the LCMS and at the interface with the plasma core. In Ref. 12 this approach was applied by considering poloidally homogeneous states. There 1D transport equations, describing the radial variation of the plasma parameters, were reduced to nonlinear algebraic equations. The results were in good agreement with the direct numerical integration of 1D equations. For example, the difference in the critical density for the radial detachment did not exceed 10%. In Ref. 25, where only radiation energy losses were taken into account by modeling of MARFE, we have demonstrated that a carefully constructed 1D model reproduces well important features of 2D solutions. This is not by chance since the method used to reduce the dimensionality of partial differential equations is close to those developed and thoroughly grounded in Ref. 26. Nevertheless, a 2D numerical simulation for the situation in question, being much more general than that considered in Ref. 25, is one of the main priorities of our future studies.

A. Transport equations

By integrating Eq. (3) with respect to x we take into account the relation $\partial\xi = \sqrt{g_{xx}}\partial x$ and Eqs. (1) and (2) with the boundary conditions (6). Since at the LCMS the influxes of neutrals is balanced by the outflow of ions and at the interface with the plasma core all particle fluxes vanish, one gets as a result,

$$\frac{\partial\langle n\rangle}{\partial t} + \frac{1}{qR}\frac{\partial\langle\Gamma_\parallel\rangle}{\partial\vartheta} = 0 \tag{9}$$

An analogous procedure performed with the parallel momentum and heat transport equations leads to

$$\frac{\partial\langle\Gamma_\parallel\rangle}{\partial t} + \frac{1}{qR}\frac{\partial}{\partial\vartheta}\left(\frac{2\langle n\rangle\langle T\rangle}{m_i}\xi_1 + \frac{\langle\Gamma_\parallel\rangle^2}{\langle n\rangle}\xi_2\right) = -\frac{\Gamma_p}{\delta_{\text{edge}}}\frac{\langle\Gamma_\parallel\rangle}{\langle n\rangle}\xi_3, \tag{10}$$

$$3\frac{\partial}{\partial t}(\langle n\rangle\langle T\rangle\xi_1) + \frac{1}{qR}\frac{\partial}{\partial\vartheta}\left[-\frac{\langle\kappa_\parallel\rangle}{qR}\frac{\partial\langle T\rangle}{\partial\vartheta}\xi_4 + \langle\Gamma_\parallel\rangle\left(5\langle T\rangle\xi_5 + m_i\frac{\langle\Gamma_\parallel\rangle^2}{\langle n\rangle^2}\xi_6\right)\right] = \frac{q_{\text{core}}/\sqrt{g_{xx}} - q_{\text{loss}}}{\delta_{\text{edge}}}, \tag{11}$$

where the dimensionless factors $\xi_1, \ldots$ are of the order of 1 and relate the averages of products with the products of averages for different plasma parameters; they are estimated on the basis of 1D modeling of radial profiles (see Refs. 12 and 21) and will be assumed, henceforth, as independent of ϑ and time; the density of energy losses from the edge region, q_{loss}, includes the contributions from different channels: impurity radiation, q_{rad}, convection of charged particles through LCMS and ionization of recycling neutrals, $q_{\text{conv/rec}} = \Gamma_p(3\langle T\rangle\xi_5 + \langle E_i\rangle\xi_6)$, and plasma heat conduction, $q_{\text{cond}} = \kappa_\perp\langle T\rangle\xi_7/\delta_T/\sqrt{g_{xx}}$.

As the next step we combine Eqs. (9) and (10) in order to reduce them to an ordinary differential equation of second order. For this reason the time derivatives are replaced by finite differences: $\partial\langle f\rangle/\partial t \approx (\langle f\rangle - \langle f\rangle_-)/\tau$, where $\langle f\rangle_- = \langle f(t-\tau)\rangle$ and τ is the time step. By integrating Eq. (9) with respect to ϑ and by taking into account that $\langle\Gamma_\parallel\rangle(0) = 0$, one obtains

$$\langle\Gamma_\parallel\rangle(\vartheta) = -\frac{qR}{\tau}N(\vartheta) \tag{12}$$

with the new variable

$$N(\vartheta) = \int_0^\vartheta (\langle n\rangle - \langle n\rangle_-)d\vartheta. \tag{13}$$

With $\langle\Gamma_\parallel\rangle$ in the form (12) and $\langle n\rangle = dN/d\vartheta + \langle n\rangle_-$, one gets from Eq. (10) an equation for N:

$$\frac{d^2N}{d\vartheta^2} + a\frac{dN}{d\vartheta} - bN + F = 0, \tag{14}$$

where

$$a = \left(\frac{d\ln\langle T\rangle}{d\vartheta} - 2M\sqrt{g\xi_3}\right)M_1, \quad b = g\left(1 + \frac{\xi_2\Gamma_p\tau}{\delta_{\text{edge}}\langle n\rangle}\right)M_1,$$

$$F = \left(gN_- + \langle n\rangle_-\frac{d\ln\langle n\rangle_-\langle T\rangle}{d\vartheta}\right)M_1, \tag{15}$$

with

$$M = \frac{\langle\Gamma_\parallel\rangle}{c_s\langle n\rangle}\sqrt{\frac{\xi_1}{\xi_2}}, \quad M_1 = 1 - M^2, \quad g = \frac{1}{\xi_1}\left(\frac{qR}{\tau c_s}\right)^2,$$

$$c_s = \sqrt{\frac{2\langle T\rangle}{m_i}}.$$

The boundary conditions to Eq. (14), $N(0)=0$ and $N(2\pi)=0$, imply the conservation of the total number of particles at the plasma edge. Together with Eq. (11), where the time derivative is replaced by the finite difference, Eq. (14) provides a set of nonlinear ordinary differential equations for N and $\langle T\rangle$. They allow us to find by iterations the poloidal distributions of these parameters, and, thus, of the physical density and parallel flux, $\langle n\rangle$ and $\langle\Gamma_\parallel\rangle$, at a given time moment with known parameters as the previous one. It is necessary to note that the procedure based on the integration of the second-order equation for N is essentially more reliable and numerically stable than the integration of two first-order equations (9) and (10) for $\langle n\rangle$ and $\langle\Gamma_\parallel\rangle$.

B. Radiation energy loss

Impurity radiation losses are dominated by locally eroded particles which are far from ionization-recombination equilibrium described normally by corona model.[27] An analytical noncorona model presented in Ref. 24 takes into account the transport of both impurity neutrals and ions under the assumption that the latter can be separated into groups of "radiant" and "dim" charge states. The former are ions with excitation energies much less than their ionization potentials. In the case of light impurities such as Be, B, and C, this group embraces the ions of low charges up to that of Li-like ones.[28] The latter includes He-and H-like ions with very high excitation energies and fully stripped impurity nuclei.

This model for impurity transport and radiation is of course highly simplified compared to a complete numerical treatment of the problem. However, it takes into account important features of such a treatment, e.g., the role of the source of neutral impurities at the wall and transport of ions in the plasma. In Ref. 24 it was demonstrated that the model reproduces well the experimentally found behavior of the impurity radiation potential with the plasma conditions in TEXTOR.[15]

We apply here the approach outlined in Ref. 24 by assuming that the radiant ions do not exist beyond the edge region. This condition takes into account the fact that outside the edge layer the electron temperature has a very sharp radial gradient and is promptly elevated to a level significantly higher than the ionization potential of Li-like particles. In Ref. 24 the "nonexistence condition" for radiant particles was imposed at the "infinite" distance from the LCMS. For the purpose of Ref. 24, the study of MARFE threshold, this difference is of minor importance, since under these conditions the temperature at the edge is high enough and radiant ions penetrate into the plasma on a distance shorter than δ_{edge}. In the present investigation we consider also the MARFE state and in the MARFE region the temperature is so low that impurity radiant species have too few chances to be ionized. Therefore a proper boundary condition for their density is very essential. According to Ref. 24, $q_{\mathrm{rad}}=j_0 E_{\mathrm{rad}}$, where j_0 is the influx of impurity neutrals related to the outflow of background ions through the erosion coefficient and E_{rad} the impurity radiation potential. With the present boundary condition we have

$$E_{\mathrm{rad}} = E^0_{\mathrm{rad}} \times \frac{l_{\mathrm{rad}}\left[1+\exp\left(-\frac{\delta_{\mathrm{edge}}}{l_0}\right)\right]\tanh\left(\frac{\delta_{\mathrm{edge}}}{2l_{\mathrm{rad}}}\right) - l_0\left[1-\exp\left(-\frac{\delta_{\mathrm{edge}}}{l_0}\right)\right]}{l_{\mathrm{rad}}-l_0}, \tag{16}$$

where $E^0_{\mathrm{rad}}=l_0/(l_{\mathrm{rad}}+l_0)\times L_{\mathrm{rad}}/k^{\mathrm{Li}}_{\mathrm{ion}}$ is the relation for the radiation potential obtained in Ref. 24 with $l_0=V_0/k^0_{\mathrm{ion}}/\langle n\rangle$ and $l_{\mathrm{rad}}=\sqrt{D_\perp/k^{\mathrm{Li}}_{\mathrm{ion}}/\langle n\rangle}$ being the penetration depths, k^0_{ion} and $k^{\mathrm{Li}}_{\mathrm{ion}}$ the ionization rates of impurity neutrals and Li-like ions, respectively; V_0 the velocity of impurity neutrals, L_{rad} the cooling rate of radiant species. In the limit case of a shallow penetration of impurity neutrals and radiant ions, $l_{\mathrm{rad}}, l_0 \ll \delta_{\mathrm{edge}}$, E_{rad} approaches E^0_{rad}; in the opposite situation, $\delta_{\mathrm{edge}} \ll l_{\mathrm{rad}}$, l_0, $E^0_{\mathrm{rad}} \approx \delta^3_{\mathrm{edge}}/(12 l_0 l^2_{\mathrm{rad}})\times L_{\mathrm{rad}}/k^{\mathrm{Li}}_{\mathrm{ion}}$.

C. Plasma particle loss

The density of the plasma particle outflow through the LCMS, Γ_p, is one of the key parameters in the 1D model for the plasma edge. According to the definition it can be estimated as follows:

$$\Gamma_p \approx \frac{D_\perp}{\sqrt{g_{xx}}}\frac{\Delta n}{\delta_{\mathrm{edge}}} \approx D_\perp \frac{\Delta n}{\delta_\xi}, \tag{17}$$

where $\Delta n \approx 2\langle n\rangle$ is the characteristic variation of the plasma density across the edge layer, and the relation between δ_ξ and δ_{edge} is derived in the Appendix. In order to assess δ_ξ we proceed from Eq. (2) where the spacial derivative is replaced with the division by the characteristic dimension. In the region where the source of hot atoms due to charge exchange of cold ones is negligible, we have

$$D_h \frac{\langle n_h\rangle}{\delta^2_\xi} \approx k_i\langle n\rangle\langle n_h\rangle - k_r\langle n\rangle^2. \tag{18}$$

The influx of hot atoms into this region, $J_h \approx 2D_h\langle n_h\rangle/\delta_\xi$, is the sum of the influxes of neutrals reflected from the wall and produced by the charge exchange of cold ones:

$$J_h \approx R_p\Gamma_p + \Gamma_p(1-R_p)\frac{k_{\mathrm{cx}}}{k_i+k_{\mathrm{cx}}}. \tag{19}$$

By combining equations above one finally gets

$$\delta_\xi \approx \frac{1}{\langle n\rangle\sigma_* \sqrt{1-k_r V_i^2/D_\perp/\langle n\rangle/k_i/(R_p k_i + k_{\mathrm{cx}})}} \tag{20}$$

where $\sigma_* = V_i/\sqrt{(k_i+k_{\mathrm{cx}})k_i}$ is the characteristic cross section for the attenuation of hydrogen neutrals in the plasma due to ionization.

D. Thermal instabilities at the edge

As it was demonstrated in Refs. 24 and 29 the plasma edge is thermally unstable if $\partial q_{\mathrm{loss}}/\partial\langle T\rangle < 0$. Indeed, when this criterion is fulfilled a spontaneous reduction of $\langle T\rangle$ would lead to an increase in the energy losses and a further reduction of the temperature. Since there are different contributions to q_{loss} different channels of instability exist.

Normally $\partial q_{\mathrm{rad}}/\partial\langle T\rangle < 0$ since the radiation potential E_{rad} increases with decreasing temperature: the lower the temperature, the longer is the lifetime of radiant impurity ions until ionization. This tendency can be, however, altered by the temperature dependence of the impurity erosion coefficient. Thus, physical sputtering increases promptly when the projectile energy exceeds a certain threshold. On the contrary, chemical erosion of carbon depends weakly on the particle energy. This difference can be one of the causes for significantly different MARFE thresholds found experimentally in TEXTOR with carbonized, boronized, and siliconized walls,[16] however, distinct recycling properties also play a very important role.[24]

Convection-recycling losses can also lead to a thermal instability.[30] Indeed, a local spontaneous reduction of the temperature leads through the pressure equilibration to an increase of the density. Therefore the perpendicular density gradient $\langle n\rangle/\delta_{\mathrm{edge}}$ grows and the loss of charge particles through the LCMS, Γ_p, increases as $\langle n\rangle^2 \sim 1/\langle T\rangle^2$. Thus, $q_{\mathrm{conv/rec}} \sim 3\xi_5/\langle T\rangle + \langle E_i\rangle\xi_6/\langle T\rangle^2$ and $\partial q_{\mathrm{conv/rec}}/\partial\langle T\rangle < 0$. Also this behavior can be essentially modified by the wall reaction. If hydrogen neutrals are released from the wall too slowly, the instability development is dragged on and cannot happen during a reasonable time. This point has been touched in Ref. 24 and will be discussed in detail elsewhere.

It is easy to see that $\partial q_{\rm cond}/\partial\langle T\rangle > 0$ and heat conduction loss plays as usual a stabilizing role. The threshold of a thermal instability is determined by the condition that the temperature dependence of $q_{\rm rad}$ and $q_{\rm conv/rec}$ overcomes that of $q_{\rm cond}$. On the one hand, both $q_{\rm rad}$ and $q_{\rm conv/rec}$ increase with the plasma density and there should be a density limit for the instability. On the other hand, $q_{\rm cond}$ varies as $1/\sqrt{g_{xx}}$ and has a minimum at the HFS. Therefore an instability starts there and this prescribes the position of MARFE.[31,25]

IV. MODEL FOR ANOMALOUS TRANSPORT COEFFICIENTS

The density of charged particle loss Γ_p, being essential for both $q_{\rm rad}$ and $q_{\rm conv/rec}$, is determined by the diffusivity $D_\perp$. In fusion devices, and especially at the plasma edge, the latter is of anomalous nature and is due to turbulence driven by diverse drift microinstabilities. Strong radial gradients of plasma parameters, collisions between electron and ions, poloidal inhomogeneity of magnetic field have been identified as possible causes for instable modes, such as drift-Alfvén (DA), drift resistive (DR), and drift resistive ballooning (DRB). Due to complexity of the problem sophisticated approaches have been developed to model the edge turbulence and realized in numerical codes such as BOUndry Turbulence (BOUT),[10] Drift ALFven 3 (DALF3),[32] Resistive Ballooning Modes 3 Dimensional (RBM3D).[33] In the present paper we assess the effect of these instability channels on anomalous transport by using a reduced semianalytical model. In spite of its relative simplicity this model reproduces in agreement with code simulations the transition to increased anomalous transport with rising density.

A. Equations for small perturbations of plasma parameters

Small perturbations of electric current $\tilde{j}$, density $\tilde{n}$, electrostatic potential $\tilde{\varphi}$, radial magnetic field $\tilde{B}_r$, and parallel electric field $\tilde{E}_\parallel$ are assumed in the form $f(l)\exp(iky-i\omega t)$, where k is the wave vector in the direction on the magnetic surface perpendicular to the field lines, ω is the complex frequency, and the envelope function f takes into account the variation of the perturbation along the magnetic field. The latter arises since the toroidal magnetic field decays with the distance R from the tokamak axis as $B=B_0R_0/R=B_0/(1-r/R_0\cos\vartheta)$, where B_0 is the magnetic field at the axis of the LCMS situated at the radius R_0. The perturbed ion velocity $\vec{V}_i$ is taken as the sum of $\vec{E}\times\vec{B}$, polarization, diamagnetic, and gyroviscous drift contributions.[34]

From the ion momentum balance equation one gets the perturbations of the current density perpendicular to the magnetic field:

$$\hat{j}_x = 2iK\hat{n},\ \hat{j}_y = -K\omega/\omega_{ci}(\hat{\varphi}+\hat{n}), \tag{21}$$

where $\hat{\vec{j}}=\tilde{\vec{j}}/j_s$, $\hat{n}=\tilde{n}/n$, $\hat{\varphi}=e\tilde{\varphi}/T$, $j_s=enc_s$, $c_s=\sqrt{T/m_i}$ is the ion sound velocity, $K=k\rho_s$, $\rho_s=c_s/\omega_{ci}$ the ion Larmor radius, $\omega_{ci}=eB/(m_ic)$ the ion Larmor frequency. By applying the plasma quasineutrality condition, $\vec{\nabla}\cdot\vec{j}=0$, we obtain for the perturbation of the parallel current component:

$$\partial\hat{j}_\parallel/\partial\vartheta = iK[4q\cos\vartheta\hat{n} + \omega\tau_s K(\hat{\varphi}+\hat{n})] \tag{22}$$

with $\tau_s=qR/c_s$. The relation between perturbations of the density and potential follows from the ion continuity equation:

$$\hat{n} = (\omega_*/\omega - K^2)/(1+K^2)\hat{\varphi} \tag{23}$$

where $\omega_*=Kc_s/L_n$ is the electron drift frequency with $L_n=dx/d\ln n$ being the density e-folding length. From the parallel component of the Faraday's law one gets

$$\tilde{B}_x/B = i(\beta/K)\hat{j}_\parallel \tag{24}$$

and from the radial component we deduce the parallel electric field

$$\tilde{E}_\parallel/E_s = i(\tau_s\omega\beta/K^2)\hat{j}_\parallel - \partial\hat{\varphi}/\partial\vartheta \tag{25}$$

with $\beta=4\pi nT/B^2$ and $E_s=T/(qRe)$.

Finally, we use the parallel electron motion equation

$$\frac{m_e}{e}\frac{d\tilde{j}_\parallel}{dt} + T\nabla_\parallel\tilde{n} + \frac{d(nT)}{dx}\frac{\tilde{B}_x}{B} = -en\tilde{E}_\parallel + \frac{m_e\nu_e}{e}\tilde{j}_\parallel, \tag{26}$$

where ν_e is the electron-ion collision frequency. With the relations obtained above one gets the following eigenfunction equation for the potential perturbation:

$$\frac{\partial^2\hat{\varphi}}{\partial\vartheta^2} = \left[\tau_s\omega\left(\frac{\beta}{M}+\frac{m_e}{m_i}M\right) + i\frac{qR}{\lambda_c}\sqrt{\frac{m_e}{m_i}}M - \beta\frac{qR}{L_P}\right]\frac{\tau_s\omega M(\omega_*+\omega)+4q(\omega_*-\omega M^2)\cos\vartheta}{\omega_*-\omega(1+2M^2)}\hat{\varphi} \tag{27}$$

with λ_c being the mean free path length of electrons between collisions with ions and $L_P=dx/d\ln(nT)$ the e-folding length of the pressure. In order to take into account the effect of the magnetic shear $s=L_n d\ln q/dr$ on drift instabilities through the Landau damping,[34] the effective perpendicular wave number $M=\sqrt{K^2+2s^2}$ has been introduced.

By inspecting Eq. (27), one can identify several combinations of terms which are responsible for different unstable modes. The first term in square brackets in combination with the first term in the numerator of the second factor ("1/1" combination) is responsible for DA modes, the "2/1" combination describes DR modes, and the "2/2" one DRB modes. The last term in square brackets is responsible for β stabilization of edge instabilities, which was considered in several papers as a trigger of L-H transition.[9,35]

B. Dispersion relation and characteristics of unstable modes

By making use of the substitution $z=(\pi-\vartheta)/2$ the eigenfunction equation (27) can be reduced to the Mathieu equation[36]

$$\partial^2\hat{\varphi}/\partial z^2 + (a-2p\cos 2z)\hat{\varphi} = 0 \tag{28}$$

with the coefficients

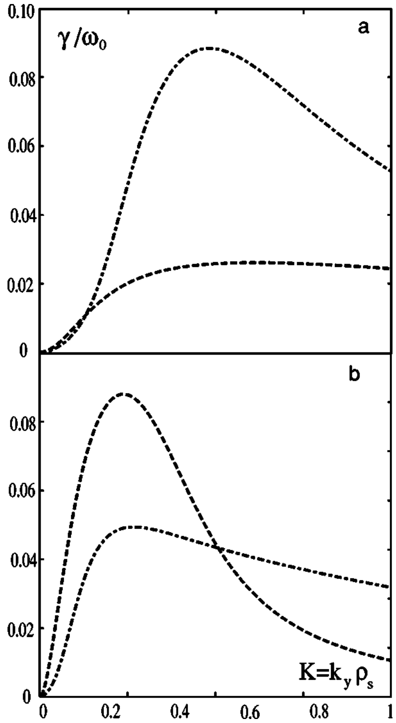

FIG. 2. The K spectra of the normalized growth rates of unstable modes with the eigenfunctions given by the zeroth-order (broken curve) and (chain curve) second-order Mathieu functions computed for edge plasma parameters in TEXTOR at low (a) and high (b) collisionality.

$$a = -\frac{4\tau_s\omega M(\omega_* + \omega)}{\omega_* - \omega(1+2M^2)}b, \quad p = -\frac{8q(\omega_* - \omega M^2)}{\omega_* - \omega(1+2M^2)}b, \tag{29}$$

where $b=\tau_s\omega[(\beta/M)+(m_e/m_i)M]+i(M/2q)\alpha_c-(\alpha/q)$, $\alpha_c=(2q^2R/\lambda_c)\sqrt{m_e/m_i}$ is the collisionality parameter related to the diamagnetic parameter α_d introduced in Ref. 9 and $\alpha=q^2R\beta/L_P$ is the MHD parameter.[9]

Equation (28) has periodic boundary conditions, but there are no terms which would require an asymmetry of eigenfunctions and we confine ourselves without loss of generality to poloidally symmetric solutions with zero derivatives at $\vartheta=0, 2\pi$. Moreover, only solutions of a period multiple to 2π with respect to ϑ are in question. These constraints restrict the multitude of solutions to even Mathieu functions of even orders, $ce_{0,2,\ldots}$. In this study, only the first two, ce_0 and ce_2, will be taken into account under the assumption that the contribution from higher orders is small. By applying approximate algebraic relations between eigenvalues a and p,[36]

$$a_0 \approx -2p^2/(p+4), \quad a_2 \approx (-2p^2+40p+128)/(p+32), \tag{30}$$

one gets dispersion relations between ω and K. Considered as equations for ω, these can be reduced to polynomial algebraic equations of the fourth and fifth order, respectively, which are solved numerically by using a standard subroutine. Only the roots of the maximum positive growth rate $\gamma=\mathrm{Im}\,\omega$ are selected and considered henceforth.

Figure 2 shows the K spectra of γ normalized to $\omega_0=c_s/L_n$, computed for TEXTOR with $a=0.46$ m, $R=1.75$ m, $B=2.25$ T, $q=3$, and two sets of parameters at the plasma edge. The first case with a relatively low density $\langle n\rangle$ of 1.5×10^{19} m^{-3}, corresponding to a collisionality factor $\alpha_c\approx0.5$. The mode represented by the second-order Mathieu function has the largest growth rate and should dominate the transport. For α_c approaching to zero, $|p|\ll1$ and ce_2 reduces to a single Fourier harmonic with $k_\parallel=1/qR$.[36] These modes coincide with those considered in Ref. 35 and being triggered by drift-Alfvén instability. For these modes the poloidal dependence of the magnetic field plays a minor role and their amplitude does not have a pronounced maximum at any particular position on the magnetic surface. Under conditions of a high plasma collisionality with $\langle n\rangle=2.5\times10^{19}$ m^{-3} and $\alpha_c\approx5$, the mode described by the zeroth-order Mathieu function has the maximum growth rate. This mode having a ballooning Gaussianlike form with a single maximum at the LFS,[36] i.e., reproduces the localization of DRB modes.

C. Anomalous diffusivity

An unstable drift mode induces a particle flux perpendicular to the magnetic surfaces with the density $\Gamma_\perp=\tilde{n}V_E^*+\text{c.c.}$,[34] where $V_E=c(-ik\tilde{\varphi})/B$ is the drift velocity due to the perturbation of the poloidal electric field. For the potential perturbation we use the quasilinear approximation[34] $|\tilde{\varphi}|\approx\gamma/k_xk_y\times B/c$. The component of the wave vector perpendicular to the magnetic surface, k_x, can be estimated as $1/x_0$, where x_0 is the radial width of the mode restricted by the magnetic shear:[34] $x_0\approx\rho_s/s$. By taking into account the relation (23), one finds the contribution of a mode to the anomalous particle diffusivity $D_\perp\equiv\Gamma_\perp n/L_n$:

$$D_\perp = \frac{\gamma^3}{\omega_r^2+\gamma^2}\left(\frac{\rho_s}{s}\right)^2\frac{2}{1+M^2}. \tag{31}$$

Figure 3 displays the K dependence of $D_\perp$ for the parameters used above by calculating the spectra in Fig. 2. One can see that the maximum contribution to the transport coefficient is normally not provided by the mode with the maximum growth rate, i.e., the wave numbers at which the growth rate and the transport contribution approach their maxima, $K^\gamma_{\max}$ and $K^D_{\max}$, respectively, do not coincide. A linear model does not take into account an interaction of different eigenmodes and cannot firmly predict which of them actually dominates the transport. This can be done only by means of a firm nonlinear consideration of the anomalous transport, e.g., by coupling with a turbulence code. Such a development is planned for future but presently we confine ourselves to the linear approach developed above. Concerning typical transport coefficients and their variation with collisionality, being most important for the present subject, this approach gives results similar to nonlinear simulations.

In order to assess how the model results are sensitive to the assumptions done, both situations with the transport governed by the modes with $K^\gamma_{\max}$ or $K^D_{\max}$ are considered. Figure 4 shows $D_\perp$ versus the collisionality parameter α_c. The discontinuity in the curve slope corresponds to the transition from the transport dominated by the Mathieu eigenmodes of the second order, ce_2, to that due to the modes of the zeroth

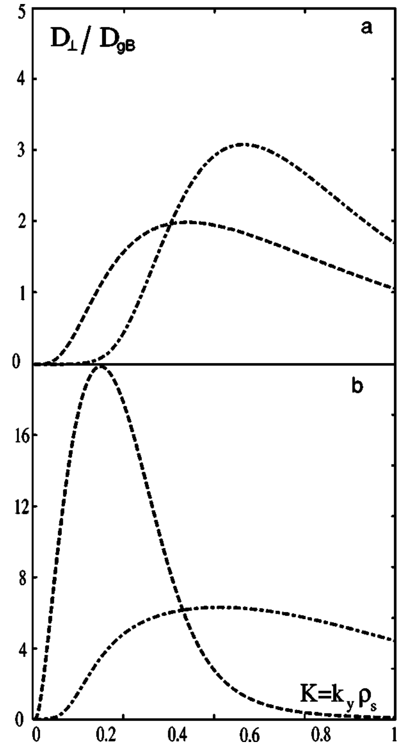

FIG. 3. The K spectra of the contributions to the particle diffusivity normalized to the gyro-Bohm coefficient $D_{gB}=c_s\rho_s^2/L_n$ from unstable modes with the eigenfunctions given by the zeroth-order (broken curve) and (chain curve) second-order Mathieu functions computed for edge plasma parameters in TEXTOR at low (a) and high (b) collisionality.

order, ce_0. The discontinuity in the dependence found with $K_{\max}^{\gamma}$ mimics the fact that for $0.8 \leqslant \alpha_c \leqslant 2$ the modes of the second order have the maximum γ but do not produce the largest transport.

According to Fig. 4, $D_\perp \approx 2D_{gB}$ if $\alpha_c \geqslant 0.2$ but is not too high and the transport is still governed by the ce_2 mode. In this range $D_\perp$ is practically independent of the magnetic field curvature and collision frequency, in agreement with the simulation results.[32] Nevertheless, the instabilities in question exist only due to collisions and $D_\perp \to 0$ when $\alpha_c \to 0$. In the range of small collisionality, $\alpha_c \leqslant 0.2$, a consideration of nonlinear effects is unavoidable for transport calculations[37]

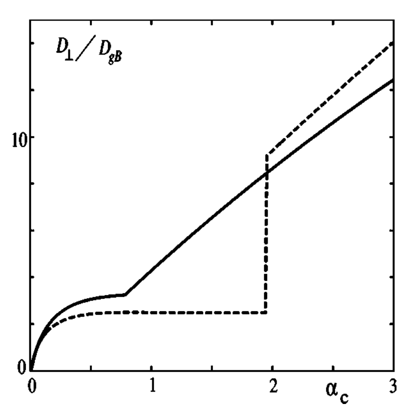

FIG. 4. Poloidally averaged values of the anomalous diffusivity computed for unstable modes with the maximum contribution to the transport (solid curve) and with the maximum growth rate (broken curve).

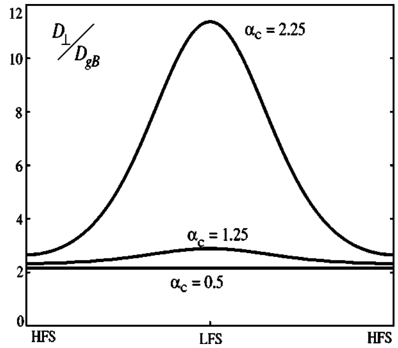

FIG. 5. Poloidal profiles of the anomalous diffusivity for different values of the collisionality parameter.

since collisionless electron drift instabilities are completely suppressed by the magnetic shear.[38,39] However, this range of parameters corresponds to low density and high temperature and is beyond the scope of the present study.

When the collisionality is high enough and $\alpha_c \gg 1$, $D_\perp \sim \alpha_c D_{gB}$ and can be reduced to the form more familiar for the DRB-induced transport:[11]

$$D_\perp \sim (q\rho_e)^2 \nu_{ei} \frac{R}{L_n}. \tag{32}$$

The poloidal dependence of particle losses, given by $|\hat{\varphi}(\vartheta)|^2$, also varies significantly with α_c when this is larger than 1. Figure 5 demonstrates $D_\perp(\vartheta)$ profiles for several values of α_c.

V. RESULTS OF COMPUTATIONS

In this section we present and qualitatively interpret the results of modeling of transitions at the plasma edge leading to the development of strong inhomogeneities, MARFE at the HFS and detachment at the LFS, and preceding the density limit.

A. Computations with prescribed transport coefficients

For these computations $D_\perp = 1m^2/s$ was assumed. Figures 6(a) and 6(b) display the stationary poloidal profiles of the average plasma density and temperature at the edge of additionally heated plasmas in TEXTOR with $P_{\text{core}} = 1.3$ MW, $d\Delta/dx = 0.25$, found for different values of the poloidally averaged density at the interface between the edge and core regions, $\overline{n} = 2\int_0^{2\pi}\langle n\rangle(d\vartheta/2\pi)$. One can see that at a critical level of $\overline{n}$ between 5 and 5.5×10^{19} m^{-3} there is a dramatic change in profiles from relatively smooth ones to those with very pronounced maximum (minimum) at the HFS. As it is observed in experiments, this modification is accompanied by a significant increase of impurity radiation from the MARFE region presented in Fig. 6(c). This increase is normally considered as an evidence of the dominant role of impurity radiation by MARFE formation. In order to check this guess, computations were performed without impurity radiation, i.e., with $q_{\text{rad}} \equiv 0$. The results presented in Fig. 7 show that this leads to an increase in the critical density by 10% only. Thus other channels of energy losses from

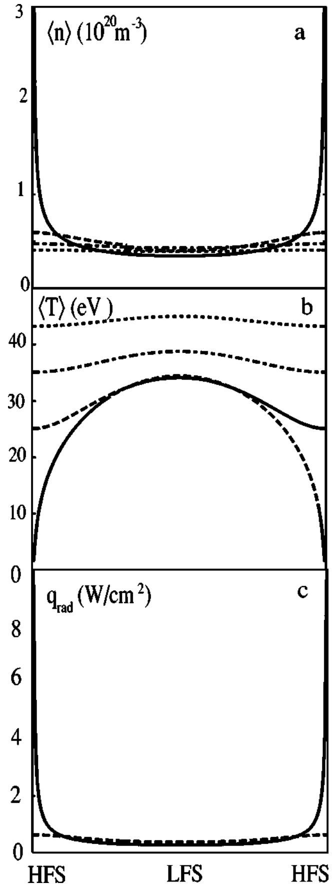

FIG. 6. Poloidal profiles of the plasma density, temperature, and energy loss with impurity radiation computed with $D_{\perp}=1\ \mathrm{m}^2/\mathrm{s}$ for different magnitudes of the poloidally averaged density $\overline{n}$: $4\times10^{19}\ \mathrm{m}^{-3}$ (points), $4.5\times10^{19}\ \mathrm{m}^{-3}$ (chain curve), $5\times10^{19}\ \mathrm{m}^{-3}$ (broken curve), and $5.5\times10^{19}\ \mathrm{m}^{-3}$ (solid curve).

the plasma edge, namely, with the plasma convection and on the ionization of recycling neutrals, are of more importance for MARFE triggering. This conclusion is in agreement with the results of our previous analysis of linear instabilities leading to MARFE (Ref. 24) and of two-dimensional computations in Ref. 40.

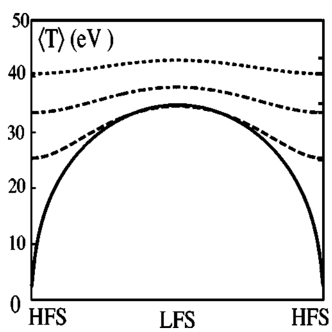

FIG. 7. Poloidal profiles of the plasma temperature computed without impurity radiation with $D_{\perp}=1\ \mathrm{m}^2/\mathrm{s}$ for $\overline{n}=4.5\times10^{19}\ \mathrm{m}^{-3}$ (points), $5\times10^{19}\ \mathrm{m}^{-3}$ (chain curve), $5.5\times10^{19}\ \mathrm{m}^{-3}$ (broken curve), and $6\times10^{19}\ \mathrm{m}^{-3}$ (solid curve).

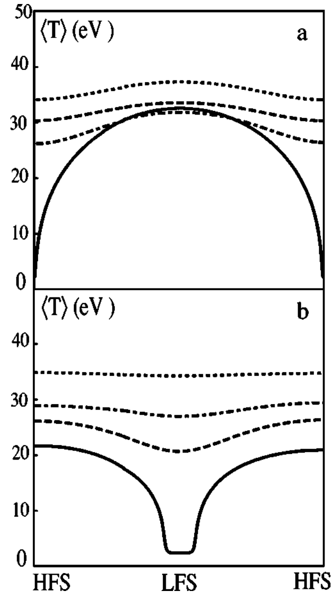

FIG. 8. Poloidal profiles of the plasma temperature computed with self-consistently determined anomalous transport coefficients: (a) for additionally heated discharges with $P_{\mathrm{core}}=1.3$ MW, $d\Delta/dx=0.25$ and $\overline{n}=4.5\times10^{19}\ \mathrm{m}^{-3}$ (points), $4.5\times10^{19}\ \mathrm{m}^{-3}$ (chain curve), $5.0\times10^{19}\ \mathrm{m}^{-3}$ (broken curve), $5.5\times10^{19}\ \mathrm{m}^{-3}$ (solid curve); (b) for ohmic discharges with $P_{\mathrm{core}}=0.3$ MW, $d\Delta/dx=0.07$ and $\overline{n}=2.5\times10^{19}\ \mathrm{m}^{-3}$ (points), $3.0\times10^{19}\ \mathrm{m}^{-3}$ (chain curve), $3.5\times10^{19}\ \mathrm{m}^{-3}$ (broken curve), $4.0\times10^{19}\ \mathrm{m}^{-3}$ (solid curve).

B. Computations with self-consistently defined transport coefficients

In the computations presented above, with prescribed diffusivity, the structure with cold dense plasma, arising when the density limit is exceeded, has always the MARFE character, i.e., it is located at the HFS, independently of the level of the poloidal asymmetry introduced by the Shafranov shift of magnetic surfaces. This fact is in agreement with our previous modeling results[25] obtained by taking into account only impurity radiation and plasma heat conduction as the energy losses from the edge. However, it is in obvious contradiction with experimental observations which show that in ohmic discharges, with reduced but finite $d\Delta/dx$ of 0.07, MARFE does not develop and a ramp up of the density to the limit results in a plasma detachment from the limiter located at the LFS.[15] This behavior can be reproduced in simulations if the model for edge anomalous transport described in the preceding section is applied. When the plasma density is high and the edge temperature is low enough, the collisionality parameter α_c exceeds 1 and the transition to the transport with pronounced ballooning character takes place. This changes the character of the poloidal asymmetry between heat influx from the core and losses from the edge due to the maximum of convective particle losses at the LFS. This can compensate or even overcome the asymmetry induced by the Shafranov shift and trigger a thermal collapse at the LFS, leading to a detachmentlike evolution of the plasma.

Figure 8 shows the results of calculations performed with the model for the edge anomalous transport described above. For the coefficients a and p in the eigenvalue equation (28) their poloidally averaged values have been used.

The transport coefficients were computed for the eigenmodes providing the largest transport, i.e., with $K=K_{\max}^{D}$. Figure 8(a) displays the stationary temperature profiles computed with the previously used relatively high level of the Shafranov shift with $d\Delta/dx=0.25$, corresponding to additionally heated discharges. As in the case of computations with prescribed diffusivity, see Fig. 6(b), MARFE formates at the HFS when a critical density is exceeded. This agrees well with experimental findings.[16] Under conditions typical for ohmic plasmas with $P_{\text{core}}=0.3$ MW and $d\Delta/dx=0.07$, see Fig. 8(b), MARFE does not develop and a region of low temperature appears at the LFS, due to the transition to the turbulence controlled by the DRB mode. In agreement with experimental data[15] the critical density is lower in this case than for additionally heated plasmas.[16]

Our calculations predict a formation of a stable state with the plasma detached at the LFS. However, in experiments a fast poloidal symmetrization normally takes place. This could be explained as follows. A strong increase of the energy losses and drop of the temperature at the LFS should lead to a local increase of the radial temperature gradient and, thus, of the density of the heat outflow from the core. Therefore, as the radial heat supply to other poloidal positions is decreased, they cool down and detachment penetrates to the HFS. Even a MARFE at the HFS may arise during this process. In the present approach with a fixed radial temperature gradient at the interface with plasma core, see Eq. (8), such a development cannot be analyzed and a further improvement of the model by taking into account the reaction of the plasma core on changes at the edge is needed.

With the transport coefficients computed for modes with $K=K_{\max}^{\gamma}$ the density threshold for the detachment increases by 15%–20% only. This change is much less than the difference in the critical α_c at which the transition to the DRB-dominated transport takes place, see Fig. 4. The cause is a very nonlinear dependence of the collisionality factor on density: $\alpha_c \sim n^{3-4}$. This results in a relatively weak sensitivity of the density threshold on the transport model assumptions

C. Discussion of results

The character of phenomena, developing at the plasma edge when the critical density is approached, is controlled by the competition of poloidal dependencies arising from the Shafranov shift of magnetic surfaces and ballooning nature of anomalous transport. One has, nevertheless, to see the principal difference between these phenomena. On the one hand, the Shafranov shift is determined by the central plasma parameters and results in a minimum at the HFS of the heat *supply* into the edge region from the plasma core. Therefore, an increase in the shift would stimulate MARFE formation. On the other hand, the ballooning character of transport results in a maximum of energy *losses* at the LFS and promotes a detachment there. These mechanisms enter into the transport equations through the poloidal variation of the metric coefficicent g_{xx} and of the transport coefficients, respectively. Qualitatively this variation can be characterized by the ratio Υ of the magnitudes of the corresponding parameters at the LFS and HFS. In the former case we have

$$\Upsilon_S = \frac{1+\Delta_1}{1-\Delta_1}$$

with $\Delta_1 = 2\times d\Delta/dx(0)$, and in the latter one

$$\Upsilon_B = \frac{|\hat{\varphi}(\pi)|^2}{|\hat{\varphi}(0)|^2} \approx \left[\frac{ce_0(\pi/2)}{ce_0(0)}\right]^2 \sim \exp(4\sqrt{|p|}).$$

In the last estimate we have accounted for the fact that the HFS/LFS assymetry in the transport arises only when the ce_0 mode is dominating and have used the relation from Ref. 36.

On the one hand, Δ_1 rises with the plasma β (Ref. 41) and, thus, Υ_S increases with the heating power. On the other hand, the factor Υ_B is controlled by the collisionality: $|p| \approx \alpha_c \sim 1/\lambda_c \sim \langle n\rangle/\langle T\rangle^2$. The temperature dependence here can be eliminated by taking into account the power balance, $\Gamma_p\langle T\rangle = D_\perp \langle n\rangle/L_n \times \langle T\rangle \sim q_{\text{core}}$. Before the onset of DRB-driven transport $D_\perp \sim D_{gB} \sim T^{3/2}/L_n$. Since the density e-folding length is determined by the penetration of neutrals, i.e., $L_n \sim 1/n$, we get $D_\perp \sim \langle T\rangle^{1.5}\langle n\rangle$, $\langle T\rangle^{2.5}\langle n\rangle^3 \sim q_{\text{core}}$, and $\alpha_c \sim \langle n\rangle^{3.4}/q_{\text{core}}^{0.8}$. For a given heating power, q_{core}, the collisionality and, hence, ballooning asymmetry increase during a density ramp up. If, nevertheless, Υ_B remains smaller than Υ_S even when the MARFE density threshold $\langle n\rangle_{\text{MARFE}}$ is approached, a MARFE will develop. Otherwise, the onset of DRB modes and detachement is more likely.

As it was demonstrated in the preceding section, the MARFE onset is essentially determined by the energy losses with the perpendicular particle convection to the inner wall. Therefore, the estimate for $\langle n\rangle_{\text{MARFE}}$, found in Ref. 6 by neglecting impurity radiation, can be applied:

$$\langle n\rangle_{\text{MARFE}} \approx \frac{1}{qR}\sqrt{\frac{\kappa_{\parallel} a}{60\pi D_\perp \sigma_*}}.$$

Here $\kappa_{\parallel} \sim \langle T\rangle^{5/2}$ and the characteristic cross section for the attenuation of hydrogen neutrals, σ_*, depends rather weakly on the electron temperature for $T \gtrsim 10$ eV. By using the estimate for $D_\perp$ and the relation between $\langle n\rangle$, $\langle T\rangle$, and q_{core} found above, we get for the plasma parameters at the MARFE onset:

$$\langle n\rangle_{\text{MARFE}} \sim q_{\text{core}}^{0.095}, \quad \langle T\rangle_{\text{MARFE}} \sim q_{\text{core}}^{0.286},$$

$$\alpha_{c,\text{MARFE}} \sim 1/q_{\text{core}}^{0.476}.$$

Thus, on the contrary to the shift asymmetry Υ_S, the ballooning asymmetry Υ_B achieved before MARFE decreases with increasing power. Therefore, MARFE develops if the heating power is above a critical level at which $\Upsilon_S = \Upsilon_B$ when $\langle n\rangle = \langle n\rangle_{\text{MARFE}}$. According to the estimate above, $\langle n\rangle_{\text{MARFE}}$ depends extremely weakly on the heating power if that exceeds the critical one. This is in agreement with experimental observations both in limiter[16] and divertor[42] machines. This fact can offer a hint why L-mode and H-mode density limits are similar despite the marked difference in heating, plasma β, and shift of magnetic surfaces, although the present model is not directly applicable to divertor conditions. For TEXTOR parameters the critical power is very close to the ohmic one. This explains why MARFE normally develops in additionally heated plasmas and detachment usually occurs under ohmic conditions.

VI. SUMMARY AND DISCUSSION

Amendments introduced into the model for the particle, momentum, and heat balances have allowed us to perform computations of the plasma parameters at the plasma edge with self-consistently described anomalous transport due to drift microinstabilities. This approach enables consideration of poloidally inhomogeneous plasma states including, e.g., the formation of MARFE at the HFS or the region at the LFS with strongly increased convective losses of particles and energy due to destabilization of drift resistive ballooning modes. It can be used to determine and predict the conditions under which the density limit is provoked either by MARFE appearance or by the transition in the edge turbulence to that driven by DRB modes. This information is of importance by elaborating methods to increase the maximum density attainable in fusion devices.

The present consideration has been done with many simplifying assumptions, e.g., about magnetic geometry, particle recycling at the LCMS, etc. The present model adequately reflects the situation in limiter devices but has to be improved in diverse respects to provide a reliable estimate for the critical density under other discharge conditions. In order to generalize the model on the case of a more relevant divertor configuration, an appropriate description of magnetic geometry with X points and of the scrape-off layer has to be included. This is necessary in order to integrate into the consideration the process of power dissipation on divertor plates discussed as an important cause of the density limit in divertor machines.[5] This modification is also unavoidable for a quantitative analysis of the effect of the plasma-wall clearance on the density limit seen in experiments on TEXTOR and Joint European Torus.[17,18]

The dynamics of the wall reaction disregarded in the present study can also be of much importance for MARFE development. If, due to specific wall properties, neutrals produced at the wall by recombination of charged particles are released into the plasma with a significant delay, MARFE appearance can be essentially dragged on. Preliminary analysis of the thermal instability threshold shows[24] that this effect may be responsible for the dependence of the density limit on the wall material properties.[16]

Finally, by solving Eq. (27) in order to estimate anomalous transport coefficients, poloidally averaged plasma parameters have been used instead of their local values. For the states with strong inhomogeneities this can lead to significant uncertainties. An amendment of the model in this respect comes up to principal difficulties and progress here may lead to important developments in the field of eigenvalue problems.

ACKNOWLEDGMENT

One of the authors (F.A.K.) is grateful for the financial support of his work by SFB 591 "Universal Behavior of Non-equilibrium Plasmas: Heating, Transport and Formation of Structures" of German Research Society.

APPENDIX: COORDINATE SYSTEM AND METRIC COEFFICIENTS

Neutral particles do not feel magnetic geometry but the charged ones are magnetized and strongly influenced by the presence of magnetic surfaces. Therefore it is convenient to introduce two coordinate systems (see Fig. 1). The one used for the description of neutrals is given by the local distance from the LCMS, ξ, and the angle ψ between the directions from the LCMS center to the point in question and to the HFS, respectively. The coordinate system used for the plasma description includes the difference x between the minor radius of the LCMS, a, and that, r, of the magnetic surface, to which the point in question belongs, and the poloidal angle ϑ, correspondingly. In a coordinate system (q^1,q^2) the square of the length element is defined as follows:[23] $(ds)^2=g_{1,1}(dq^1)^2+2g_{1,2}dq^1dq^2+g_{2,2}(q^2)^2$, and in the cylindrical coordinate system (R,Z), $(ds)^2=(dR)^2+(dZ)^2$. By taking into account the relations between coordinates

$$R = R_0 - (a-\xi)\cos\psi, \quad Z = (a-\xi)\sin\psi$$

and

$$R = R_0 + \Delta - (a-x)\cos\vartheta, \quad Z = (a-x)\sin\vartheta$$

one finds the metric coefficients $g_{\xi\xi}=1$ and $g_{xx}\approx 1+2(d\Delta/dx)\cos\theta$ where the conditions $\xi,x,\Delta \ll a, d\Delta/dx \ll 1$ were taken into account. With the same accuracy $\partial\xi/\partial x \approx 1+(d\Delta/dx)\cos\theta$ and, thus, $\delta_{\text{edge}}=\delta_x \approx \delta_\xi/[1+(d\Delta/dx)\cos\theta]$.

[1] M. Greenwald, Plasma Phys. Controlled Fusion **44**, R27 (2002).
[2] Y. Shimomura, R. Aymar, V. A. Chuyanov *et al.* Nucl. Fusion **41**, 309 (2001).
[3] N. Ohyabu, Nucl. Fusion **19**, 1491 (1979).
[4] B. Lipschultz, B. LaBombard, E. S. Marmar *et al.*, Nucl. Fusion **24**, 977 (1984).
[5] K. Borrass, R. Schneider, and R. Farengoet, Nucl. Fusion **37**, 523 (1997).
[6] M. Z. Tokar, J. Rapp, D. Reiser, U. Samm, F. C. Schüller, G. Sergienko, and P. C. de Vries, J. Nucl. Mater. **266-269**, 958 (1999).
[7] M. Greenwald, J. L. Terry, S. M. Wolfe, S. Ejima, M. G. Bell, S. M. Kaye, and G. H. Neilson, Nucl. Fusion **21**, 2199 (1988).
[8] D. L. Brower, C. X. Yu, R. V. Bravenec *et al.* Phys. Rev. Lett. **67**, 200 (1991).
[9] B. N. Rogers, J. F. Drake, and A. Zeiler, Phys. Rev. Lett. **81**, 4396 (1998).
[10] X. Q. Xu, W. M. Nevins, T. D. Rognlien, R. H. Bulmer, M. Greenwald, A. Mahdavi, L. D. Pearlstein, and P. Snyder, Phys. Plasmas **10**, 1773 (2003).
[11] P. N. Guzdar, J. F. Drake, D. McCarthy, A. B. Hassam, and C. S. Liu, Phys. Fluids B **5**, 3712 (1993).
[12] M. Z. Tokar, Phys. Rev. Lett. **91**, 095001 (2003).
[13] R. Singh, C. V. S. Rao, R. Avinash, S. P. Deshpande, and P. K. Kaw, Nucl. Fusion **32**, 379 (1992).
[14] R. Goswami, R. Singh, and P. Kaw, Phys. Plasmas **7**, 2477 (2000).
[15] U. Samm, P. Bogen, H. A. Claassen, H. Gerhauser, H. Hartwig, E. Hintz, Y. T. Lie, A. Pospieszczyk, D. Rusbüldt, and B. Schweer, J. Nucl. Mater. **176&177**, 273 (1990).
[16] J. Rapp, W. Biel, H. Gerhauser *et al.*, J. Nucl. Mater. **290-293**, 1148 (2001).
[17] P. C. de Vries, J. Rapp, F. C. Schüller, and M. Z. Tokar', Phys. Rev. Lett. **80**, 3519 (1998).
[18] J. Rapp, A. Huber, L. C. Ingesson, S. Jachmich, G. F. Matthews, V. Philipps, and R. Pitts, J. Nucl. Mater. **313**, 524 (2003).
[19] B. Lehnert, Nucl. Fusion **8**, 173 (1968).
[20] M. Z. Tokar, Plasma Phys. Controlled Fusion **35**, 1119 (1993).

[21]M. Z. Tokar, Plasma Phys. Controlled Fusion **36**, 1819 (1994).
[22]M. Z. Tokar, M. Kobayashi, and Y. Feng, Phys. Plasmas **11**, 4610 (2004).
[23]R. Balescu, *Transport Processes in Plasmas* (North-Holland, Amsterdam, 1988), Vol. 2, p. 795.
[24]M. Z. Tokar and F. A. Kelly, Phys. Plasmas **10**, 4378 (2003).
[25]M. Z. Tokar, Phys. Plasmas **9**, 1646 (2002).
[26]L. W. Kantorowitsch and W. I. Krylow, *Näherungsmethoden der Höhenanalysis* (Deutscher Verlag der Wissenschaften, Berlin, 1956), p. 282.
[27]D. E. Post, R. V. Jensen, C. B. Tarter, W. H. Grasberger, and W. A. Lokke, At. Data Nucl. Data Tables **20**, 397 (1977).
[28]X. Bonnin, R. Marchand, and R. K. Janev, At. Plasma-Mater. Interact. Data Fusion **2**, 117 (1992).
[29]M. Z. Tokar, Phys. Plasmas **7**, 2432 (2000).
[30]M. Z. Tokar, Phys. Scr. **31**, 411 (1985).
[31]M. Z. Tokar, Phys. Plasmas **8**, 2866 (2001).
[32]B. Scott, Plasma Phys. Controlled Fusion **39**, 471 (1997).
[33]P. Beyer, X. Garbet, S. Benkadda, P. Ghendrih, and Y. Sarazin, Plasma Phys. Controlled Fusion **44**, 2167 (2002).
[34]J. Weiland, *Collective Modes in Inhomogeneous Plasma* (Institute of Physics, Bristol, 2000).
[35]W. Kerner, Yu. Igitkhanov, G. Janeschitz, and O. Pogutse, Contrib. Plasma Phys. **38**, 118 (1998).
[36]*Handbook of Mathematical Functions*, edited by M. Abramowitz and I. A. Stegun (Dover, New York, 1970), p. 722.
[37]B. D. Scott, Phys. Rev. Lett. **65**, 3289 (1990).
[38]D. W. Ross and S. M. Mahajan, Phys. Rev. Lett. **40**, 324 (1978).
[39]K. T. Tsang, P. J. Catto, J. C. Whitson, and J. Smith, Phys. Rev. Lett. **40**, 327 (1978).
[40]R. Zagorski and H. Gerhauser, Phys. Scr. **70**, 173 (2004).
[41]J. Wesson, *Tokamaks*, 2nd ed. (Claredon, Oxford, 1997).
[42]T. W. Petrie, A. G. Kellman, and M. A. Mahdavi, Nucl. Fusion **33**, 929 (1993).